Available online at www.sciencedirect.com
ScienceDirect
Trans. Nonferrous Met. Soc. China 29(2019) 1824−1835
Transactions of Nonferrous Metals Society of China
www.tnmsc.cn

Effect of tool tilt angle on strength and microstructural characteristics of friction stir welded lap joints of AA2014-T6 aluminum alloy

C. RAJENDRAN[1], K. SRINIVASAN[2], V. BALASUBRAMANIAN[2], H. BALAJI[3], P. SELVARAJ[3]

1. Department of Mechanical Engineering, Sri Krishna College of Engineering and Technology, Coimbatore Tamil Nadu 641008, India;
2. Center for Materials Joining and Research (CEMAJOR), Annamalai University, Tamil Nadu 608002, India;
3. Aeronautical Development Agency, Bangalore, Karnataka 560017, India

Received 16 November 2018; accepted 15 July 2019

Abstract: Friction stir welding (FSW) has been extensively adopted to fabricate aluminium alloy joints by incorporating various welding parameters that include welding speed, rotational speed, diameters of shoulder and pin and tool tilt angle. FSW parameters significantly affect the weld strength. Tool tilt angle is one of the significant process parameters among the weld parameters. The present study focused on the effect of tool tilt angle on strength of friction stir lap welding of AA2014-T6 aluminium alloy. The tool tilt angle was varied between 0° and 4° with an equal increment of 1°. Other process parameters were kept constant. Macrostructure and microstructure analysis, microhardness measurement, scanning electron micrograph, transmission electron micrograph and energy dispersive spectroscopy analysis were performed to evaluate the lap shear strength of friction stir lap welded joint. Results proved that, defect-free weld joint was obtained while using a tool tilt angle of 1° to 3°. However, sound joints were welded using a tool tilt angle of 2°, which had the maximum lap shear strength of 14.42 kN and microhardness of HV 132. The joints welded using tool tilt angles of 1° and 3° yielded inferior lap shear strength due to unbalanced material flow in the weld region during FSW.

Key words: AA2014 aluminium alloy; friction stir lap welding; tool tilt angle; lap shear strength; microstructure

1 Introduction

Copper-containing aluminium alloys such as 2xxx and 7xxx series are most preferred while manufacturing aircraft fuselage and wing skins [1] for achieving the required strength ratio. Often, the structures are conventionally joined by rivets, bolts, nuts and screws [2] as they are prone to the formation of an oxide layer (Al_2O_3) which results in welding difficulties such as solidification cracking and porosity while using fusion welding processes. To alleviate such weld difficulties, solid-state welding process was developed [3,4]. Friction stir welding (FSW) is now successfully applied to welding these alloys for aircraft application of lap joint configuration. The substitution of fastening joints with FSW decreased the weight reduction of aircraft structures by providing fuel efficiency [5]. Apart from FSW process and tool parameters, the lap shear strength (LSS) of friction stir lap welded joints is predominantly influenced by certain factors. Such factors include hook height, hook width, stir zone area and effective sheet thickness (combined thickness of both top and bottom sheet). Lap welding between two sheets results in the formation of oxide layer. This oxide layer may enter into the stir zone no matter the chosen proper process and tool parameters. ABHIJIT et al [6] studied the impact of tool tilt angle (TA) with two pin geometries on mechanical and metallurgical properties of friction stir welded (FSWed) AA6061-T6 aluminium alloy. They observed that an increase in TA showed a significant increase in thrust and forging forces at the interface (tool–work piece). Using taper thread tool, the mean grain size decreased while TA increased. LONG et al [7] established a thermo-mechanical finite element model to analyze the thermal gradient, material flow and levelness of stress during FSW. They found a wormhole defect in the weld at 0° TA and no-defect when the tool axis was titled to 2° TA. A CFD model was proposed to investigate the effect of TA in a heating and cooling cycle and the following observations were made: (i) the maximum temperature was observed by tilted tool on the

Corresponding author: C. RAJENDRAN; Tel: +91-9865432576; E-mail: crdrn12@yahoo.com
DOI: 10.1016/S1003-6326(19)65090-9

advancing side, (ii) the tilted tool generated a higher frictional force at the interface (tool shoulder and work piece), and (iii) the tilted tool generated a stronger stirring action to the material in the vicinity of welding tool, which was beneficial to better material mixing and formation of defect free welds [8]. SHANAVAS et al [9] studied the effect of different tool pin geometries on mechanical and metallurgical properties of the FSWed AA5051-H32 aluminium alloy. The researchers found that the stir zone grains were fine and equiaxed at a TA of 1.5°, when the weld was made with tapered square threaded pin [10]. YAEMPHUAN et al [11] reported the shear strength and location of fracture of dissimilar AA6063 aluminium alloy and SUS430 stainless steel lap joint. They found that the shear strength was influenced by TA, where the tensile shear strength of lap weld increased at a TA from 0° to 2°, but at a TA beyond 2°, the strength decreased drastically.

From the earlier research work [1−11], it was found that extensive research has been performed to find the effect of TA of friction stir welded butt joints of aluminium alloys. However, to the best knowledge of the authors, limited studies have been conducted to study the influence of TA on the mechanical properties of friction stir welded lap joints of aluminium alloys. Therefore, in this study, an attempt has been made to investigate the effect of TA on the microstructure and tensile properties (lap shear strength) of friction stir welded lap joints of AA2014 aluminium alloy.

2 Experimental

AA2014-T6 aluminium alloy sheet with a thickness of 2 mm was used as test material for performing friction stir lap welding (FSLW). The chemical composition and mechanical properties of base material (BM) are presented in Tables 1 and 2, respectively. Figure 1(a) represents the FSLW configuration. The microstructure of BM is composed of grains that are coarse and elongated and are oriented along the rolling direction (Fig. 1(b)) with the average grain size of 30 μm. The tool used in this work is M2 grade high speed steel and its chemical composition is listed in Table 3. All the TA joints were made using a non-consumable tool which had a left hand thread taper tool pin profile with a shoulder diameter of 12 mm and constant pin diameter of 4 mm (Fig. 1(c)). Trial runs were carried out for five distinct TAs, viz., 0°, 1°, 2°, 3°, and 4°, and other process parameters such as tool rotation speed, traverse speed, shoulder and pin diameters and axial load are kept as constant (Table 4).

Figure 1(d) shows the photograph of fabricated FSLW joints with various TAs. The joints were first inspected visually (from front to back) and then subjected to microstructure examination, lap shear test and microhardness test to quantify the LSS. The metallography specimens were prepared by mechanically grinding, polishing with different grades of sandpapers followed by alumina powder. Subsequently, the specimens were etched by Keller's reagent and swabbed on the cross-section of the weld for microstructure analysis. Composite lap shear specimens were prepared as per the ASME/AWS/SAE/D8.9−97 standards [12]. Three specimens were tested for each condition to check the consistency of LSS (Figs. 1(e) and (f)). Microhardness measurement was performed using 0.5 mm indenter at a load of 50 N and a dwell time of 15 s along the transverse cross-section of the weld. Transmission electron microscope (TEM) was employed to evolve the precipitate size, shape and distribution in the weld region. A sample with a diameter of 3 mm was taken from the weld and subjected to a fine polishing with thickness up to 10 μm. Further, the thickness of disk was reduced noticeably by performing electro polishing. The samples were examined using high resolution-TEM (Phillips CM 12 microscope) operated at 200 kV. However, energy dispersive spectroscopy (EDS) analysis

Table 1 Chemical composition of base material AA2014-T6 (wt.%)

Si	Fe	Cu	Mn	Mg	Zn	Cr	Ti	Al
0.87	0.13	4.81	0.81	0.73	0.06	0.005	0.01	92.4

Table 2 Mechanical properties of base material AA2014-T6

Yield strength/MPa	Ultimate tensile strength/MPa	Elongation in 50 mm gauge length/%	Microhardness at 0.5 N and 15 s (HV)	Lap shear strength (LSS)/kN
432	456	10.1	161	17

Table 3 Chemical composition of high speed steel (HSS) tool material (designation to AISI: M2) (wt.%)

C	V	W	Cr	Mo	Fe
0.08	2.0	6.5	4.3	5.0	Bal.

Table 4 FSW process parameters

Process parameter	Value
Tool rotational speed/($r\cdot min^{-1}$)	900
Welding speed/($mm\cdot min^{-1}$)	90
Tool shoulder diameter/mm	18
Tool pin diameter/mm	6
Tool tilt angle/(°)	0, 1, 2, 3 and 4
Pin type	Left hand threaded tapper cylindrical pin
Shoulder concavity/(°)	1

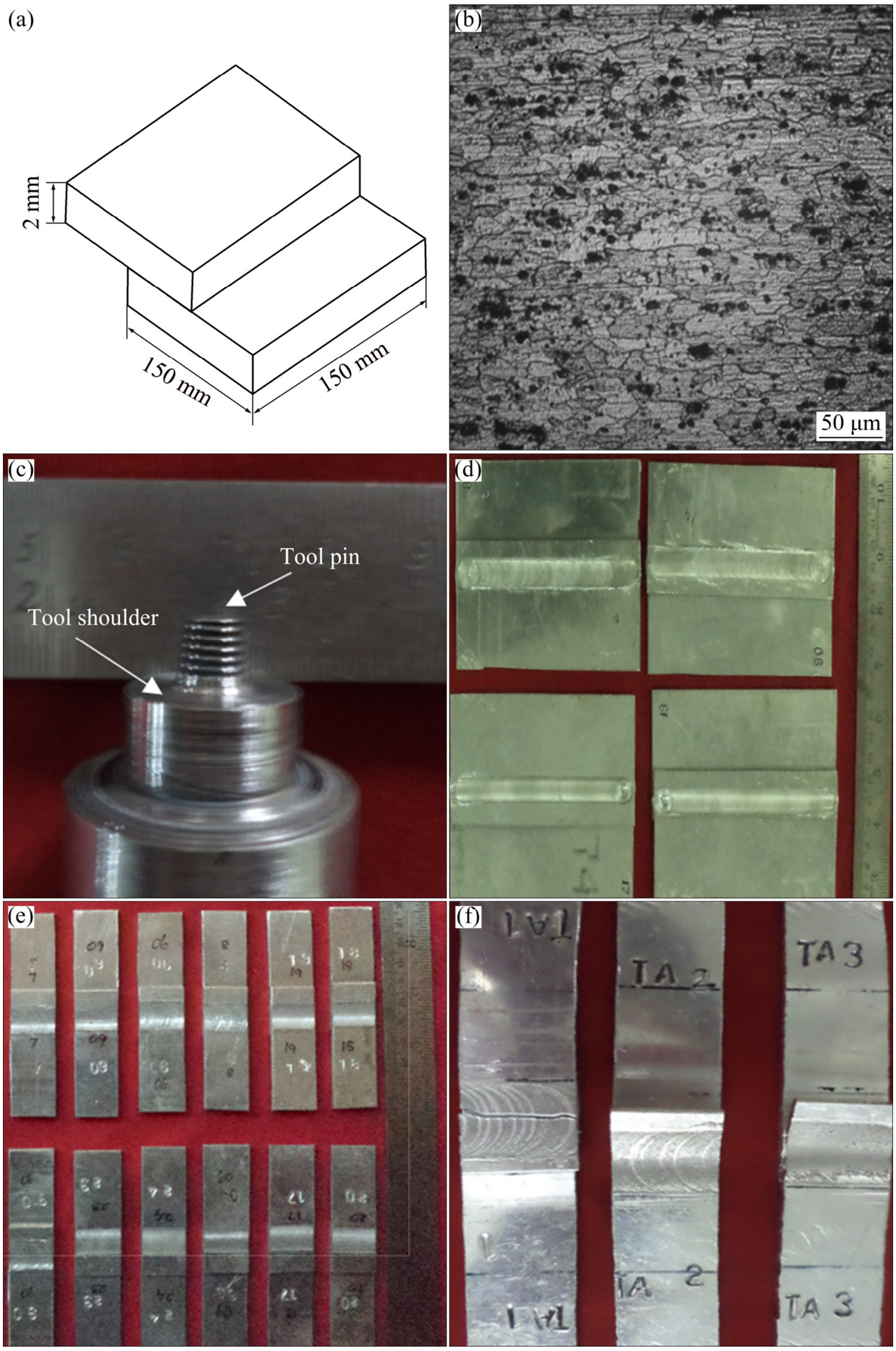

Fig. 1 Schematic diagram of lap configuration (a), optical micrograph of BM (b), photographs of tool used for FSLW (c) and fabricated FSLW joints with various TAs (d), and lap shear specimens before (e) and after (f) testing

was used to identify the chemical composition of precipitates evolved in the weld at different TAs. The joint efficiency (η) of FSLW joints under lap shear loading was calculated using Eq. (1) proposed by CEDEQVIST and REYNOLDS [13]:

$$\eta = \frac{P_1}{P_2} \times 100\%$$

where P_1 is the weld failure load (kN) and P_2 is the base material failure load (kN).

3 Results and discussion

3.1 Weld appearance

Figure 2 shows the surface appearance of welded joints produced at different TAs (0°−4°). The surface appearance of joints welded with 1°−3° TA yields defect-free and smooth surface. Fine and coarse ripples are observed on the outside (top surface) of welds. The mechanical shanking effect caused by the imbalance of stress state of the plasticized material during a change in axial force of the TA is responsible for the formation of coarse ripples [14]. There are some surface defects in the FSLW joints fabricated at low and high TAs. The process, which can explain the effect of TA in an FSWed joint, is the frictional heat generated by sliding action of the tool shoulder against the work piece, which will cause the conversion of cold material into the plasticized material. The joints are fabricated using the entire length of the sheet due to the forging of plasticized materials that develops welds. Thus, the joint is formed through forging the plastically deformed material into the joint line that creates behind the tool from the advancing side to the retreating side. As a result of decreasing TA, insufficient material flow [15] is caused in the SZ and the weld cannot be made (Figs. 3(a) and (c)). Perhaps, the gap at the tool work interface is increased by increasing the TA (3°−4°). By increasing the TA, the processed material escapes easily at the tool−work piece interface. Thus, a lack of unity occurs in the weld region that results in the development of voids. It can be seen in the joint welded at a TA of 4° (Figs. 3(b) and (d)) that lack of deformed materials on the retreating side and increasing TA enable excessive flash from the bottom of the tool [16].

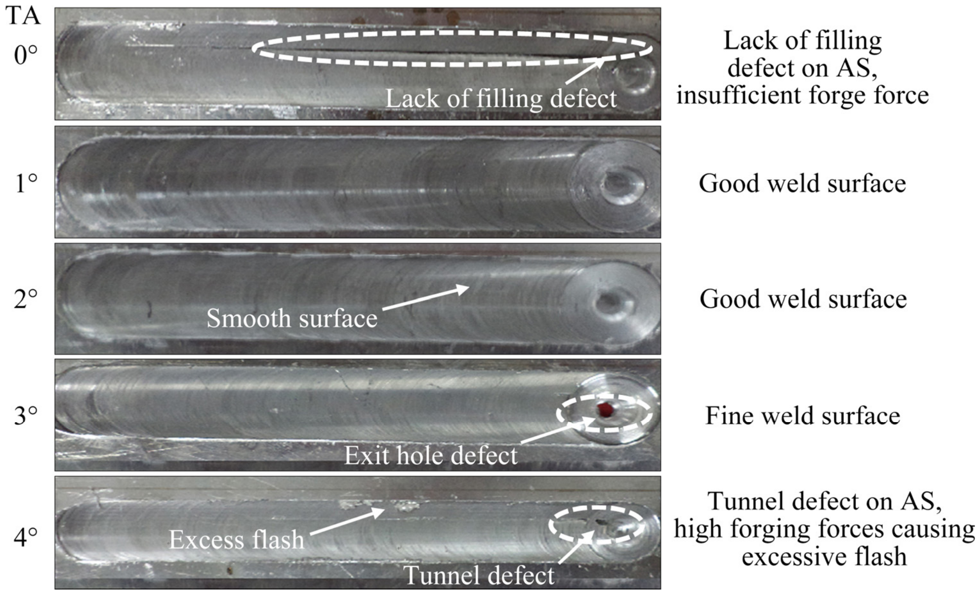

Fig. 2 Surface appearance of FSLW joints at different TAs

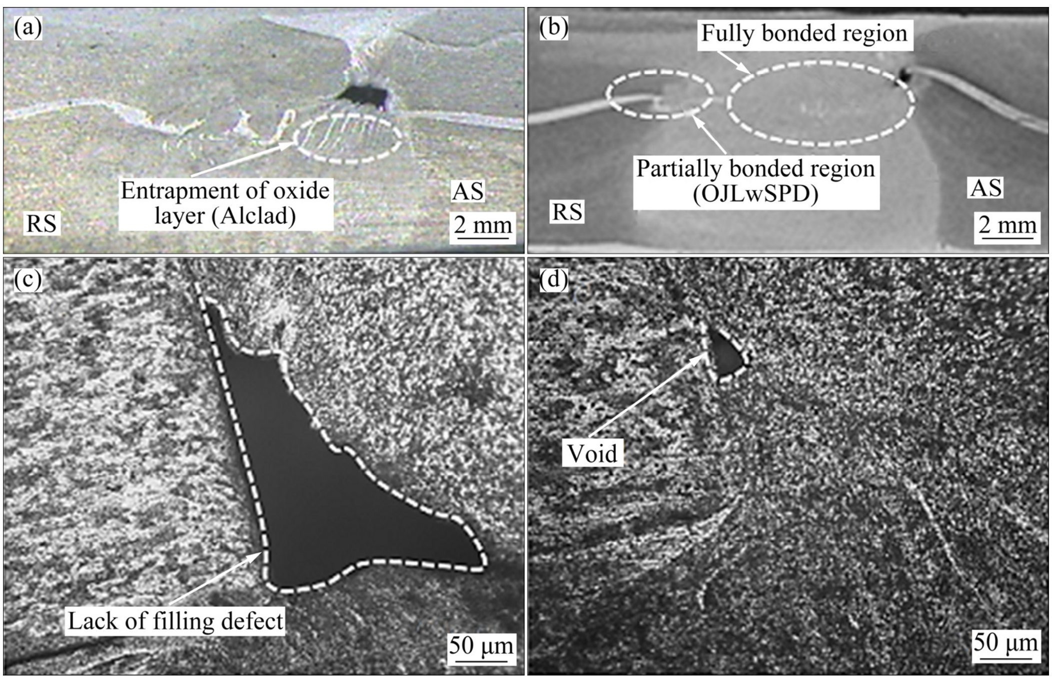

Fig. 3 Macrographs of FSLW joints at TAs of 1° (a) and 4° (b), and stir zone micrographs of welded joint at TAs of 1° (c) and 4° (d)

3.2 Macrograph

The FSLW joints are characterized into four regions such as thermo-mechanically affected zone (TMAZ), heat-affected zone (HAZ), stir zone (SZ) and BM. Table 5 illustrates the geometrical features of SZ at different TAs. It is observed that the joint fabricated using 1° TA achieved a hook height, combined thickness and SZ area of 0.03 mm, 1.71 mm and 7.2 mm^2, respectively. Similarly, hook height, combined thickness and SZ area of 0.03 mm, 1.81 mm and 8.2 mm^2 respectively are observed for the joint fabricated using 2° TA. The joint formed by 3° TA had a hook height of 0.02 mm, combined thickness of 1.73 mm and SZ area of 9.3 mm^2. The formation of SZ under different TAs is a function of temperature and material flow. Based on material flow in FSW, it is segregated into three types such as insufficient material flow, balanced material flow and turbulent material flow [17,18]. However, CHEN et al [19] observed three types of effect while using thread pin in-process material flow. Firstly, the thread pin results in improving the strain rate and velocity of material flow. Secondly, the thread pin supplies material in the high velocity zone of the thread groove opening. Thirdly, the thread pin offers vertical pressure gradient. From Fig. 3, the lack of filling defect is identified on the retreating side in the joint welded using low TA (0°). Tunnel defect is observed in the joints fabricated using high TA (4°) on retreating side. The lack of filling defect is perceived on the surface of the weld made using 0° TA, due to the insufficient deformed material around the pin. At high tool tilted position in the joint, tunnel defect is observed, which is associated with material escaped between tool and work piece interface.

In contrast, defect-free joints are observed on the retreating side at TAs from 1° to 3°. Also size and shape of SZ are changed with an increase in tool inclination with respect to work piece. In addition, the TA increasing from 1° to 3° increases the heat generation and forging force [8,9]. The forging force can be increased by increasing TA and thread pin also speeds up more volume of deformed material and thrusts the material in the downward direction [10]. However, the joint made using 4° TA causes a thinning effect (thickness reduction in top sheet) in the processed region. Hence, the combined thickness is reduced and results in lower weld strength. This is caused due to the space between the work piece and tool from the tool tilt by increasing TA. Therefore, with an increase in TA, the processed material escapes easily from the lowest part of the tool shoulder [11]. Subsequently, lack of filling occurs in the weld, which results in discontinuity on the surface. Therefore, the range of TA from 1° to 3° can be used for further investigation.

Another important criterion in FSLW is that the SZ is categorized into two regions, namely partially bonded region and fully bonded region [12]. Both regions are formed in the shoulder influencing region. These two regions are essential in FSLW. The partially bonded region is the region that is formed when both the top and bottom sheets are mated with each other. A thin layer separates it, which is formed on both sides of the shoulder region and extended toward the SZ. This line is termed as an originally joint line with severe plastic deformation (OJLwSPD) [20], kissing bond line [21] and interface [22]. During this investigation, the joint welded to 1° TA, partially bonded region is observed and extended up to SZ on the retreating side. Whereas in 2° TA joint, this region is terminated at the TMAZ/SZ interface on both advancing and retreating sides. In 3° TA joint, this region is extended up to SZ on retreating side. The extension of partially bonded region to SZ is the critical factor which causes crack initiation during tensile loading. This region may be controlled by stirring action of thread tool pin and shoulder. Hence, the joint fabricated using 2° TA yielded a maximum LSS due to the balanced material flow. In contrast, for the joint made by 1° and 3° TAs, insufficient material flow and turbulent flow result in improper hook height. Hence, these two joints yield lower strength than the joint made by 2° TA. Whereas for the fully bonded region in SZ, in which both the sheets metallurgically bonded with each other [23,24], there is no bright contrast line.

Table 5 Characteristics of FSLW Joints at different TAs

TA/(°)	Macrostructure	Hook height (HH)/mm	Effective sheet thickness (EST)/mm	Stir zone area (SZA)/mm^2	Microhardness at 0.5 N and 15 s (HV)	LSS/kN	Failure location	Probable reason
1	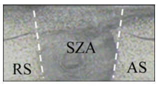	0.03	1.71	7.2	128	12.60	SZ	Insufficient material flow
2	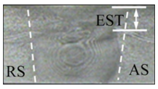	0.03	1.81	8.2	132	14.42	TMAZ/SZ	Balanced material flow
3	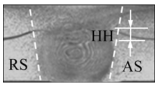	0.02	1.73	9.3	129	13.10	TMAZ/SZ	Turbulent material flow

3.3 Microstructure

Typical microstructures in distinct regions of FSLW joints welded using discrete TAs (1°−3°) are shown in Fig. 4. Figures 4(a)−(c) depict the microstructures of SZ fabricated under various TAs (1°−3°). All the SZs extensively contain equiaxed and fine grains followed by dynamic recrystallization [13,25], which could be obtained by thermo-mechanical action of tool and axial force during the FSW. Moreover, an onion ring pattern is observed in all the SZs uniformly. The formation of an onion ring in the SZ is as a result of downward and upward flow of material around the pin when the tool rotates in the favorable direction. The thread pin has positive effect to supply deformed material in the high velocity zone of the groove opening and promotes the formation of circles around the pin and along with vertical pressure gradient [12,19]. Moreover, a thread on the pin may accelerate the amount of plasticized material in the SZ for a given set of condition. Hence, the weld made with 1° TA exhibits a number of concentric circles in an onion ring region (ORR) in the SZ. Besides, the SZ conceives finer grains at recrystallized temperature of

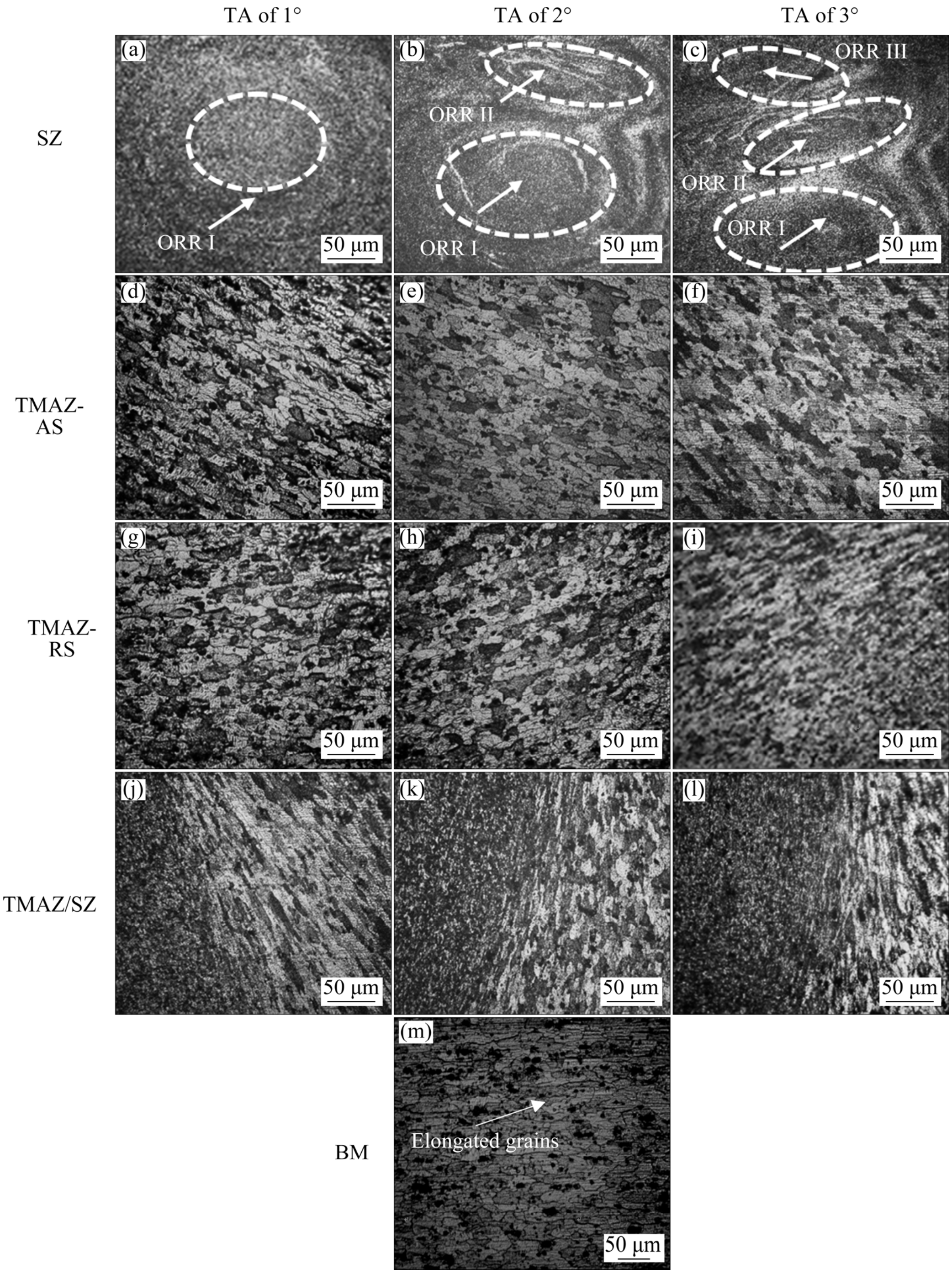

Fig. 4 Micrographs of FSLW joints at different TAs

250−450 °C and fine distribution of oxide layer in the SZ is obtained. As a result of the increase in TA, an increase in axial force and good consolidation are observed.

For 2° TA joint, the SZ shows two ORRs with a number of concentric circles, which are arranged one over by another and the area of SZ (8.2 mm^2) increases considerably. It is noted that the tool tilt position has a direct relationship with axial force which results in more heat [26]. This indicates that the SZ is subjected to severe plastic deformation. In addition, the SZ of joint fabricated with 3° TA (Fig. 4(c)) exhibits three ORRs and many numbers of concentric circles one over by another. Moreover, the SZ area is increased to 9.3 mm^2 with an increase in the axial load. But the effective sheet thickness is reduced to 1.73 mm due to partial amount of plasticized material expelled in form of flash by the rotation of tool shoulder [27,28].

The grains in the TMAZ strongly distort and partial dynamic recrystallization occurs on both sides. At various tool tilt positions, the micrograph of TMAZ on advancing side reveals coarse and elongated grains, which are formed due to the imparted stress formed due to the rotation of tool shoulder and transverse movement of the tool during the welding cycle (Figs. 4(d−f)); whereas the microstructure of TMAZ on the retreating side contains the BM microstructure because the temperature on the advancing side of TMAZ is lower due to the velocity gradient. The morphology of grains in TMAZ on retreating side shows an increase in tool tilt position and an increase in grain size gradually, which are caused by higher axial forces. Hence, the grain size in TMAZ of joint welded with higher TA of 3° capitulates coarse and elongated grains (Fig. 4(i)). Microstructure at TMAZ/SZ interface with varying TA shows a mixed flow pattern (Figs. 4(j−l)). Besides, a clear boundary is observed between the TMAZ and SZ. Among three microstructures, the micrograph of the joint welded at 2° TA has no much variation at TMAZ/SZ interface (Fig. 4(k)); whereas the other two joints (1° and 3°) have a quite variation at TMAZ/SZ interface due to the difference in velocity gradient. From the microstructural observation, it is noted that the joint welded using 2° TA offers finer grains (Fig. 4(b)) in the SZ and smoother diffusion at TMAZ/SZ interface on both sides than other joints. This is attributed to a balanced material flow, optimal heat input and good consolidation of deformed material in the weld.

3.4 Lap shear strength and fracture location

The LSS values of joints welded using different TAs are presented in Table 5, which is lower than the BM failure load (17 kN, see Table 2). The joints welded using 1°, 2° and 3° TAs offer the maximum LSS values of 12.60, 14.42 and 13.10 kN, respectively. From Table 5, the joint made using 2° TA conceives a maximum LSS of 14.42 kN, which is 15% inferior to that of BM failure load. Low variation in LSS is attained for TAs of 1°−3°. High LSS of 14.42 kN is observed for TA of 2°. This may be associated to the steady flow of material in the SZ, caused by an optimum hook height of 0.03 mm, effective sheet thickness of 1.81 mm and SZ area of 8.2 mm^2. Thus, the SZ is formed by an upward and downward flow of material between two sheets and sufficient axial force to fill the weld defects [29,30]. The other joints (1° and 3° TAs) exhibit lower LSS due to the redistributed aluminum cladding (Alclad). The Alclad layer penetrates into the SZ, which promotes crack propagation path during tensile loading as it is much softer than aluminium alloy. Therefore, the morphology of redistributed Alclad layer in the SZ significantly influences the strength of FSLW joints, as shown in Figs. 4(a−c).

Higher TA redistributed Alclad disperses more obviously in the SZ and this prevents the redistributed Alclad from creating a crack propagation line during tensile loading (Fig. 4(c)). 90% of fracture path in FSW occurs at the interface of TMAZ/SZ on the advancing side. This is due to thermal softening and grain coarsening during the thermal cycle. In the weld made using 1° TA, the fracture occurs in the SZ due to lower consolidation because the lower tool tilt position produces less heat inception and minimum forging force [31,32]. The fracture location of FSLW made using 3° TA is on advancing side of top sheet and retreating side of lower sheet because the lower sheet on retreating side is more prone to failure than upper sheet on advancing side.

Figure 5 reveals the SEM fractographs of broken joints to show the mode of fracture. Under the higher magnification, the fractured regions contain fine and shallow dimples with populated voids with varying shape and size that are scattered across the transgranular fracture region. This reveals that fracture mode is ductile. SEM fractographs of joint at low TA show coarse dimples with few straight ridges (Fig. 5(a)). It may be attributed to insufficient heat input for grain recrystallization and uniform distribution of Alclad layer. Whereas, the 2° TA joint exhibits fine dimples with a population of voids with variation in size and shape. Furthermore, the distribution of Alclad layer is uniform in the fracture region, which is attributed to sufficient heat generated for the recrystallization of grains and uniform distribution of Alclad layer. Besides, the joint made using higher TA reveals fine dimples with some coarse precipitates of various sizes. It may be associated with higher heat input by changing tool tilt position and axial force. Hence, the joint fabricated using 2° TA yields higher LSS than the other welded joints.

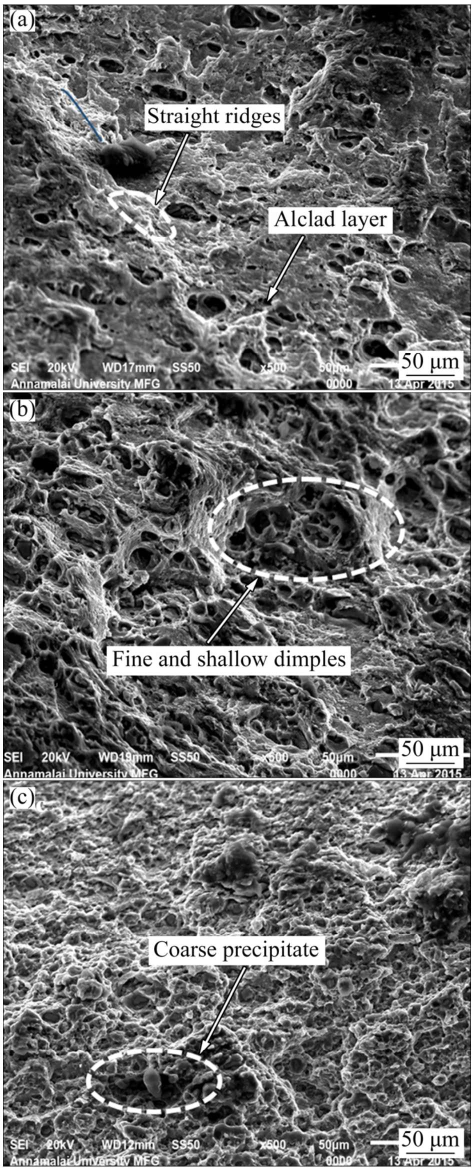

Fig. 5 SEM fractographs of FSLW joints using different TAs: (a) 1°; (b) 2°; (c) 3°

3.5 Microhardness

Hardness distribution of FSLW joints fabricated using various TAs (1°−3°) is shown in Fig. 6. The mechanical properties of joint are mainly dependent upon the thermal cycle during FSW. They would be greatly affected by the properties of precipitates like size, shape and distribution [33,34]. The FSW joints experienced severe plastic deformation followed by dynamic recrystallization in the SZ. Also, the average microhardness values of SZ are presented in Table 5. In addition, the maximum hardness of HV 132 is observed in the weld made by 2° TA. It is also perceived that the hardness in SZ increases with increasing TA from 1° to 2°. This is due to the formation of fine and recrystallized grains and the density distribution of precipitates in the SZ. However, two lowest hardness distribution regions are observed at TMAZ/SZ interface on both advancing and retreating sides, which are caused by the dissolution or coarsening of strengthening precipitates due to peak temperature. The precipitates would be coarsened at 300−400 °C and dissolve above 505 °C [35]. Moreover, the HAZ is not affected very much during the thermal cycle and retains the same microstructure, and no alteration is observed.

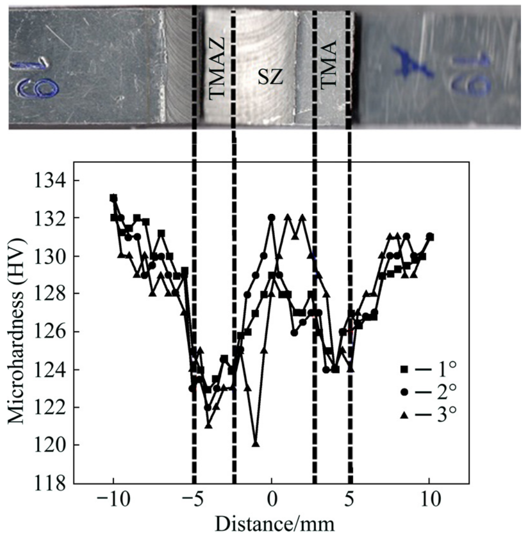

Fig. 6 Microhardness distribution of FSLW joints

Precipitates play a vital role in the precipitation hardening of aluminum alloy. The precipitates act as an obstacle for dislocation during tensile loading. Hence, it is responsible for improving the strength and hardness of aluminum alloy. The second phase particles initially presented in the base material get fragmented into small particles due to severe plastic deformation occurring in the SZ. In FSW, the heating and cooling in the weld during the thermal cycle are similar to the aging process. The variation in hardness with different TAs exhibits different hardness peaks [36−38]. From Fig. 6, the joint welded using 1° TA conceives a maximum hardness of HV 128 in the SZ. Nevertheless, the peak hardness in the SZ is achieved by the formation of GP-I zone (coherent with aluminum matrix).

Furthermore, increasing TA from 1° to 2° improves the hardness property and a maximum hardness of HV 132 is observed in the SZ. By the precipitation of second phase θ'' (GP-II zone) and θ' particle (metastable), definite crystal structure and maximum hardness are improved in the SZ. Temperature increases with increasing TA from 2° to 3°. Hence, the SZ subjected to severe heat input results in a gradual decline in hardness value in the SZ due to coarsening of precipitate by over aging. The SZ experiences thermal cycle with peak temperature between 410 and 550 °C during FS. In addition, the materials are softened because of either coarsening of continued cooling time or precipitation of incoherent stable precipitate (equilibrium θ phase formed and coherency strain lost). There is an impulse for the small particle to solve and the resultant solute produces more copious precipitates, which causes them to grow, thereby lowering interfacial energy. This process is named as particle coarsening. Hence, the joint welded using 2° TA offers higher hardness than other joints due to the formation of θ'' and θ' precipitates. Al−Cu is the binary aluminum alloy and has an inevitable natural aging process. The equation shows that the sequence of precipitation from solid solution is as follows [39]:

$$\alpha_{sss} \longrightarrow \underset{\text{(Cu-rich phase)}}{GP_2\ \text{zone}} \longrightarrow \underset{\text{(Metastable)}}{\theta''} \longrightarrow \underset{\text{(Metastable with definite crystal structure)}}{\theta'} \longrightarrow \theta(CuAl_2)$$

The over aging zone offers the lowest hardness distribution for the TMAZ or HAZ. This region experiences a thermal cycle with a peak temperature between 200 and 410 °C during FSW [40]. It is noted that all the low hardness regions experienced thermal cycle with the same peak temperature of 360−370 °C during the FSW of AA6061 [41] and 340 °C for FSW of AA2024 aluminium alloy. It is inferred that the FSLW under different TAs experienced similar thermal cycle, resulting in coarsening of $CuAl_2$ precipitates and the formation of a lower hardness distribution region on both advancing and retreating sides. Even though the coarsening level of the precipitate depends on the aging time at 180 °C, increasing the TA would increase the aging time of Al_2Cu precipitate. The TA is direct proportional to the aging time. Hence, the joint fabricated using higher TA results in high aging time, which promotes coarse precipitate with the lowest hardness. The aging process is the way for obtaining the lowest hardness distribution region found in all tool tilted welds.

3.6 TEM micrograph

The BM is composed of fine needle-like and spherical shape precipitates in the T6 condition. Figures 7(a−d) depict the TEM micrographs of BM and SZ. These micrographs reveal coarse and fine precipitates of

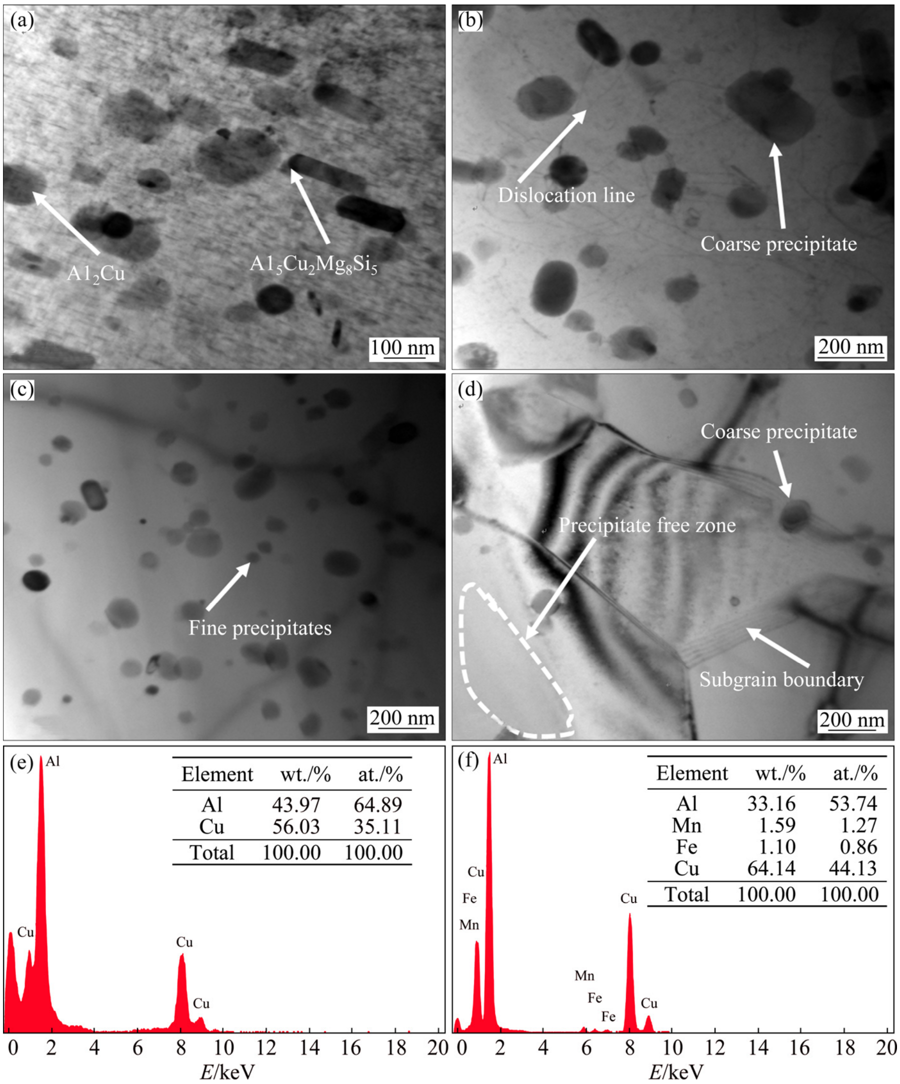

Fig. 7 TEM micrographs of base material (a), SZs of FSLW joints using TAs of 1° (b), 2° (c) and 3° (d) and EDS analysis of coarse (e) and fine (f) precipitates in SZ

$CuAl_2$ which are observed by TEM with EDS analysis (Fig. 7(e)) [32−44]. It is understood that the coarse precipitates are composed of $CuAl_2$ and the fine precipitates $Al_5Cu_2Mg_8Si_5$ consisting of Al, Cu, Mg and Si [12]. The strengthening precipitates appear in two sizes, which are coarse and fine precipitates. The average size of coarse precipitates varies from 50 to 100 nm. In contrast, the average size of fine precipitates varies from 10 to 50 nm. The size and shape of precipitates in the weld zone depend on thermal cycle. Coarse precipitates contain fragments of several particles and fine precipitates may be dissolved in the weld. Figures 7(b−d) show the TEM micrographs of SZ fabricated using different TAs, which reveal the precipitates of various sizes formed due to the peak temperature developed in the weld. As the TA increases, the heat input and consolidation of material increase due to the forging force. The increase in TA enhances the dissolution of precipitates as well as the formation of coarse precipitate. The SZ of weld joint produced using 1° TA contains fine precipitate except for some coarse precipitates. This indicates that the fragment of coarse precipitates is lower due to lower forging force. The SZ of joint welded using 2° TA shows a uniform distribution of precipitates by an optimum forging force in the weld zone.

In contrast, the joint made using 3° TA angle shows coarse and uneven distribution of precipitates in the SZ. It is inferred that the SZ is subjected to severe heat input during the welding cycle. As a result, the heat dissipation is reduced and it takes long time to dissipate the heat. It promotes large precipitate by re-precipitation of precipitates. From the EDS analysis (Fig. 7(f)), the joint fabricated using 2° TA shows the formation of the second phase particle, which has a combination of Al, Cu, Fe and Mn. This may be due to the formation of $(CuFeMn)Al_6$ precipitates [45,46]. It is the main reason for the joint yielded the maximum LSS as observed in the joint welded using 2° TA. During FSW, 3° TA makes precipitate-free zone with coarse precipitate (50−100 nm). The formation of precipitate-free zone and coarse precipitate in the SZ is due to the thermal driving force that increases cooling time and reduces fine precipitates by grain coarsening mechanism. As a result of higher TA (3°), the weld region subjected to severe friction causes high heat input by excess forging of tool. Hence, high heat input in the SZ does not benefit FSW and reduces the LSS of FSLW joints.

4 Conclusions

(1) The friction stir lap welding of AA2014-T6 aluminum alloy can be successfully realized using the tilt angles of 1°−3°.

(2) The joint welded using a tilt angle of 2° yielded a maximum lap shear strength of 14.42 kN and exhibited a maximum efficiency of 84%; the joint welded using tilt angles of 1° and 3° exhibited inferior lap shear strength due to the unbalanced material flow in the weld region during FSW.

(3) The thread tool pin is an important factor to control the material flow behavior on the formation of sound welded joints.

(4) The formation of closely spaced onion rings, finer grains and higher hardness (HV 132) in the stir zone offered higher lap shear strength of joints welded using a tilt angle of 2° compared with other welded joints.

(5) A joint welded using a tilt angle of 2° shows an optimal hook height of 0.03 mm, effective sheet thickness of 1.81 mm and stir zone area of 8.2 mm^2.

(6) Sound joints are conceived by fine and uniform distribution of strengthening precipitates of $CuAl_2$ and $(CuFeMn)Al_6$.

(7) Aluminium cladding (Alclad) layer is considered as one of the most important structures of AA2014 as it prevents the formation of corrosion. As a result of performing FSW, this aluminium cladding layer is removed and causes corrosion in the weld region due to the dispersion of Al_2O_3. This is considered as one of the limitations of this study. In order to avoid this effect, powder coating process can be deployed to improve its corrosive property.

Acknowledgements

The authors wish to record their sincere thanks to Aeronautical Development Agency (ADA), Bangalore, India, for the financial support to carry out this investigation through an R&D project No: FSED 83.07.03

References

[1] THOMAS W M, NICHOLAS E D, NEEDHAM J C, MURCH M G, TEMPLESMITH P, DAWES C J. Improvements relating to friction welding: European patent, 0615480B1[P]. 1992−11−27.

[2] NANDAN R, DEBROY T, BHADSHIA H K D H. Recent advances in friction stir welding-process, weldment structure and properties [J]. Progress in Material Science, 2008, 53: 980−1023.

[3] MISHRA R M, MAHONEY M W. Friction stir welding and processing [M]. Ohio: ASM International, 2007: 360.

[4] TERRY K. An outsider looks at friction stir welding (ANM-112N-05-06) [R]. 2005. https://www.faa.gov/aircraft/air_cert/design_approvals/csta/publications/media/friction_stir_welding.pdf.

[5] WILLIAMS S W. Welding of airframes using friction stir welding [J]. Air Space Europe, 2001, 3(3−4): 64−66.

[6] ABHIJIT B, BARNIK S R, JOHN D B, SUBHASH S C. An experimental investigation of torque and force generation for varying tool tilt angles and their effects on microstructure and mechanical properties: Friction stir welding of AA6061-T6 [J]. Journal of Manufacturing Process, 2018, 31: 395−404.

[7] LONG Ling, CHEN Gao-qiang, ZHANG Shuai, LIU Tie, SHI Qing-yu. Finite-element analysis of the tool tilt angle effect on the formation of friction stir welds [J]. Journal of Manufacturing Processes, 2017, 30: 562−569.

[8] ZHANG Shuai, SHI Qing-yu, LIU Qu, XIE Rui-shan, ZHANG Gong, CHEN Gao-qiang. Effects of tool tilt angle on the in-process heat transfer and mass transfer during friction stir welding [J]. International Journal of Heat and Mass Transfer, 2018, 125: 32−42.

[9] SHANAVAS S, EDWIN RAJA DHAS J, PAULO DAVIM J. Effect of geometry of tool pin profile on the mechanical and metallographic characteristics of friction stir welded AA5052-H32 aluminium alloy [J]. Journal of Manufacturing Technology Research, 2017, 9(1−2): 81−93.

[10] MOSTAFA M E, AHMED Y S, SHASH TAMER Y M, MAHMOUD ABD RABBOU S. Effect of friction stir welding parameters on the peak temperature and the mechanical properties of aluminum alloy 5083-O [J]. Improved Performance of Materials, 2017, 72: 11−25.

[11] PAIBOON Y, SURAT T, KITTIPONG K. Shear strength and fracture location of dissimilar A6063 aluminum alloy and SUS430 stainless steel lap joint [J]. Applied Mechanics and Materials, 2018, 773: 196−201.

[12] BABU S, JANAKIRAM G D, VENKATAKRISHNAN P V, MADHUSUDHANA REDDY G, PRASADRAO K. Microstructure and mechanical properties of friction stir lap welded aluminum alloy AA2014 [J]. Material Science and Technology, 2012, 28(5): 414−426.

[13] CEDEQVIST L, REYNOLDS A P. Factors affecting the properties of friction stir lap joints [J]. Welding Journal, 2001, 80(s): 281−287.

[14] BOZKURT Y, SALMAN S, CAM G. Effect of welding parameters on lap shear tensile properties of dissimilar friction stir spot welded AA5754-H22/2024-T3 joints [J]. Science and Technology of Welding and Joining, 2013, 18(4): 337−345.

[15] CHEN Hua-bin, YAN Keng, LIN Tao, CHEN Shan-ben, JIANG Cheng-yu, ZHAO Yong. The investigation of typical welding defects for 5456 aluminum alloy friction stir welds [J]. Material Science and Engineering A, 2006, 433(1−2): 64−69.

[16] SHULTZ E F, COLE E G, SMITH C B, ZINN M R, FERRIER N J, PFEFFERKORN F E. Effect of compliance and travel angle on friction stir welding with gaps [J]. Journal of Manufacturing Science and Engineering, 2010, 132(4): 041010-9.

[17] LIU H J, ZHANG H J, YU L. Effect of welding speed on microstructures and mechanical properties of underwater friction stir welded 2219 aluminum alloy [J]. Materials & Design, 2011, 32: 1548−1553.

[18] KUMAR K, SATISH K V. The role of friction stir welding tool on material flow and weld formation [J]. Materials Science and Engineering A, 2008, 485: 367−374.

[19] CHEN Gao-qiang, LI Han, ZHANG Shuai, DAI Qi-lei, WANG Xi-bo, ZHANG Gong, SHI Qing-yu. Effects of pin thread on the in-process material flow behavior during friction stir welding: A computational fluid dynamics study [J]. International Journal of Machine Tools Manufactures, 2018, 124: 12−21.

[20] CAO X, JAHAZI M. Effect of tool rotational speed and probe length on lap joint quality of a friction stir welded magnesium alloy [J]. Materials & Design, 2011, 32: 1−11.

[21] DUBOURG L, MERATI A, JAHAZI M. Process optimization and mechanical properties of friction stir lap welds of 7075-T6 stringers on 2024-T3 Skin [J]. Materials & Design, 2010, 31: 3324−3330.

[22] CANTIN G M D, DAVID S A, CURZIO E L, BABU S, THOMAS W M. Microstructural characteristics and mechanical properties of friction skew stir welded lap joints in 5083-O aluminum [C]// Proceedings of the 7th International Conference on Trends in Welding Research Pine Mountain. Georgia, USA, ASM International, 2005: 185.

[23] ZHANG Gui-feng, SU Wei, ZHANG Jun, WEI Zhong-xin, ZHANG Jian-xun. Effects of shoulder on interfacial bonding during friction stir lap welding of aluminum thin sheets using tool without pin [J]. Transactions of Nonferrous Metals Society of China, 2010, 20(12): 2223−2228.

[24] BARLAS Z. The influence of tool tilt angle on 1050 aluminum lap joint in friction stir welding process [J]. Acta Physica Polanica A, 2017, 132: 679−681.

[25] YANG Min, BAO Rui-jun, LIU Xiu-zhong, SONG Chao-qun. Thermo-mechanical interaction between aluminum alloy and tools with different profiles during friction stir welding [J]. Transactions of Nonferrous Metals Society of China, 2019, 29(3): 495−506.

[26] MAJID E, HAMED A D, MORTEZA H. Investigations of tool tilt angle on properties friction stir welding of A441AISI to AA1100 aluminium [J]. Journal of Engineering Manufacture, 2016, 230(7): 1234−1241.

[27] SURESH D M, MADHUSUDHAN R G. Influence of tool tilt angle on material flow and defect generation in friction stir welding of AA2219 [J]. Defence Science Journal, 2018, 68(5): 512−518.

[28] NARGES D, MIGUEL C, MICHELE C. Effect of the tool tilt angle on the heat generation and the material flow in friction stir welding [J]. Metals, 2019, 9(1): 1−17.

[29] NANDAN R, DEBROY T, BADHESHIA H K D H. Recent advances in friction stir welding process, weldment structure and properties [J]. Progress in Materials Science, 2008, 53: 980−1023.

[30] MUHAYAT N, ZUBAYDI A, SULISTIJONO YULIADIM Z. Effect of tool tilt angle and tool plunge depth on mechanical properties of friction stir welded AA5083 joints [J]. Applied Mechanics and Materials, 2014, 493: 709−714.

[31] KUSH P, MEHTA A, VISHVESH J, BADHEKA A. Effects of tilt angle on properties of dissimilar friction stir welding copper to aluminum [J]. Materials and Manufacturing Process, 2014, 31(3): 255−263.

[32] RESHAD SEIGHALANI K, BESHARATI GIVI M K, NASIRI A M, BAHEMMAT P. Investigations on the effects of the tool material, geometry and tilt angle on friction stir welding of pure titanium [J]. Material Engineering and Performance, 2010, 19: 955−96.

[33] KRISHNAN K N. On the formation of onion rings in friction stir welds [J]. Material Science and Engineering A, 2002, 327: 246−251.

[34] RAMANJEYANUL U, MADHUSUDHANA R, HINA. Optimization of process parameters of aluminium alloy AA2014-T6 friction welds by response surface methodology [J]. Defence Technology, 2015, 11: 209−219.

[35] NANDAN R, DEBROY T, BADHESHIA H K D H. Recent advances in friction stir welding process, weldment structure and properties [J]. Progress in Material Science, 2008: 53, 980−1023.

[36] HAD H, ROSLEE A A. Study on the role of friction stir welding tilt angle on microstructure and hardness [J]. Applied Mechanics and Materials, 2015, 799−800: 434−438.

[37] SAFARBALI B, SHAMANIAN M, ESLAMI A. Effect of post-weld heat treatment on joint properties of dissimilar friction stir welded 2024-T4 and 7075-T6 aluminum alloys [J]. Transactions of Nonferrous Metals Society of China, 2018, 28(7): 1287−1297.

[38] RAJENDRAN C, SRINIVASAN K, BALASUBRAMANIAN V, BALAJI H, SELVARAJ P. Evaluation of load-carrying capabilities of friction stir welded, TIG welded and riveted joints of AA2014-T6 aluminium alloy [J]. Aircraft Engineering and Aerospace Technology, 2019. doi.org/10.1108/AEAT-11-2017-0233.

[39] LORIMER G W. Precipitation processes in solids [M]. Warrendale: TMS-AIME, 1978: 87.

[40] XU W F, LIU J H, LUAN G H, DONG C L. Microstructure and mechanical properties of friction stir welded joints in 2219-T6 aluminum alloy [J]. Materials & Design, 2009, 30(9): 3460−3467.

[41] FULLER C B, MAHONEY M W, CALABRESE M, MICONA L. Evolution of microstructure and mechanical properties in naturally aged 7050 and 7075 Al friction stir welds [J]. Material Science and Engineering A, 2010, 527(9): 2233−2240.
[42] GÜREL Ç, SELCUK M. Recent developments in friction stir welding of Al-alloys [J]. Materials Engineering and Performance, 2014, 23(6): 1936−195.
[43] LEE W B, YEON Y M, JUNG S B. Evaluation of the microstructure and mechanical properties of friction stir welded 6005 aluminum alloy [J]. Materials Science and Technology, 2003, 19(11): 1513−1518.
[44] HATTINGH D G, BLIGNAULT C, VANNIEKERK T I, JAMES M N. Characterization of the influences of FSW tool geometry on welding forces and weld tensile strength using an instrumented tool [J]. Journal of Materials Processing Technology, 2008, 203(1−3): 46−57.
[45] MONDOLFLO L F. Aluminum alloy structures and properties [M]. London: Butterworth, 1976.
[46] BROOKS C R. Heat treatment structures and properties of non-ferrous alloy [M]. Ohio: ASM, Metalparks, 1984.

搅拌头倾斜角对搅拌摩擦焊 AA2014-T6 铝合金焊接接头强度和显微组织的影响

C. RAJENDRAN[1], K. SRINIVASAN[2], V. BALASUBRAMANIAN[2], H. BALAJI[3], P. SELVARAJ[3]

1. Department of Mechanical Engineering, Sri Krishna College of Engineering and Technology, Coimbatore Tamil Nadu 641008, India;
2. Center for Materials Joining and Research (CEMAJOR), Annamalai University, Tamil Nadu 608002, India;
3. Aeronautical Development Agency, Bangalore, Karnataka 560017, India

摘　要：结合各种焊接参数，包括焊接速度、转速、轴肩和搅拌针直径、搅拌头倾斜角等，搅拌摩擦焊(FSW)已经广泛应用于制造铝合金接头。FSW 参数能够显著影响焊接强度，其中，搅拌头倾斜角是一种重要的过程参数。因此，本文作者研究搅拌头倾斜角对搅拌摩擦焊铝合金(AA2014-T6)搭接焊接强度的影响。搅拌头倾斜角的变化范围为 0°~ 4°，等值增量为 1°，其他参数保持一致。采用宏观和微观组织分析、显微硬度测量、扫描电镜、透射电镜和能谱分析等方法对搅拌摩擦搭接接头的搭接剪切强度进行测定。结果表明，当搅拌头倾斜角为 1°~3°时，可获得无缺陷的焊接接头；当倾斜角为 2°时，可获得具有最大剪切强度(14.42 kN)和显微硬度(HV 132)的接头。采用 1°和 3°倾斜角焊接的接头其剪切强度较差，这是搅拌摩擦焊过程中焊接区域内物料流动不平衡导致的。

关键词：AA2014 铝合金；搅拌摩擦搭接焊；搅拌头倾斜角；搭接剪切强度；显微组织

(Edited by Wei-ping CHEN)